Oxygen-atom substitution in a β-ketoenamine-linked covalent organic framework for boosting photocatalytic oxygenation of sulfides

Hongxiang Zhao , Yuexin Wang , Fulin Zhang , Xiaoyun Dong , Xianjun Lang [*]

Hubei Key Lab on Organic and Polymeric Optoelectronic Materials, College of Chemistry and Molecular Sciences, Wuhan University, Wuhan 430072, China

ARTICLE INFO

ABSTRACT

Covalent organic frameworks (COFs), a class of crystalline porous materials, have been widely adopted as visible light photocatalysts. Benzothiadiazole is a prevalent building block for COFs, and oxygen-atom substitution of the sulfur-atom of benzothiadiazole leads to benzooxadiazole. Here, with pyrrolidine as the catalyst, two highly crystalline β-ketoenamine-linked COFs, TpBTD-COF and TpBO-COF, are synthesized by the condensation of 1,3,5-triformylphloroglucinol (Tp) with 4,4′-(benzothiadiazole-4,7-diyl)dianiline (BTD) and 4,4′-(benzooxadiazole-4,7-diyl)dianiline (BO), respectively. As such, TpBO-COF exhibits augmented visible light absorption and accelerated charge separation and transport compared with TpBTD-COF based on detailed optical and photoelectrochemical characterizations. Moreover, both TpBTD-COF and TpBO-COF can speedily promote selective oxygenation of sulfides with TEMPO as the hole transfer mediator irradiated by blue light. TpBO-COF exhibits higher activity than TpBTD-COF for the oxygenation of sulfides to sulfoxides with dioxygen. This work demonstrates that heteroatom substitution into COFs can boost the photocatalytic activity for selective organic transformations.

1. Introduction

The increasing energy demands and exacerbating environmental pollutions have become a nonnegligible issue that hinders sustainable development [1]. Realizing the effective utilization of the most abundant clean energy, solar energy, is one of the most important ways to overcome current challenges toward future development [2,3]. Through processes of light harvesting and energy conversion, photocatalysis has received general interest in promising applications like water splitting [4–6], carbon dioxide reduction [7,8], and organic transformation [9, 10]. However, the low light utilization efficiency and poor cycling stability are challenges of current photocatalysts need to be overcome, and the overall activity still has a significant gap toward practical applications [11–13]. Therefore, it is imperative to design efficient visible light photocatalysts, exploring their structure–property relationship to boost stability and activity [14–21]. As an emerging class of crystalline organic porous materials, covalent organic frameworks (COFs) have gradually demonstrated great potential as visible light photocatalysts [22–24].

Coventionally, COFs are designed and synthesized by dynamic covalent reactions between organic building blocks [25–29]. Many

attractive advantages, such as stable covalent bonds, tunable pores and channels, and well-ordered π-stacking layers, endow COFs with characteristics of excellent charge transport efficiency, high chemical stability, and adequate active sites [30–34]. Additionally, COFs of boosted photocatalytic activity can be obtained by introducing various photoactive building units into COFs or modifying key active units [35–38]. By tuning the band structures of COFs, it is possible to propel the occurrence of specific photocatalytic reactions [39,40]. Benefiting from these favorable attributes, COFs have been steadily developed for various attractive applications in photocatalysis [41–43].

The prevailing strategy to boost the photocatalytic activity of COFs is integrating electron-withdrawing and electron-donating building blocks into the frameworks of donor–acceptor structures [44–47], leading to changes to the overall electronic environment of COFs. The organic building blocks can be customized to obtain different heteroatom-incorporated building blocks [48,49]. By integrating suitable heteroatom-incorporated building blocks into COFs to achieve heteroatom substitution, the adjustments of COFs are predicable. Introducing conjugated heterocycles can improve the optoelectronic properties of organic materials [50,51]. For example, benzothiadiazole has been integrated into many narrow bandgap materials; the improved

* Corresponding author.
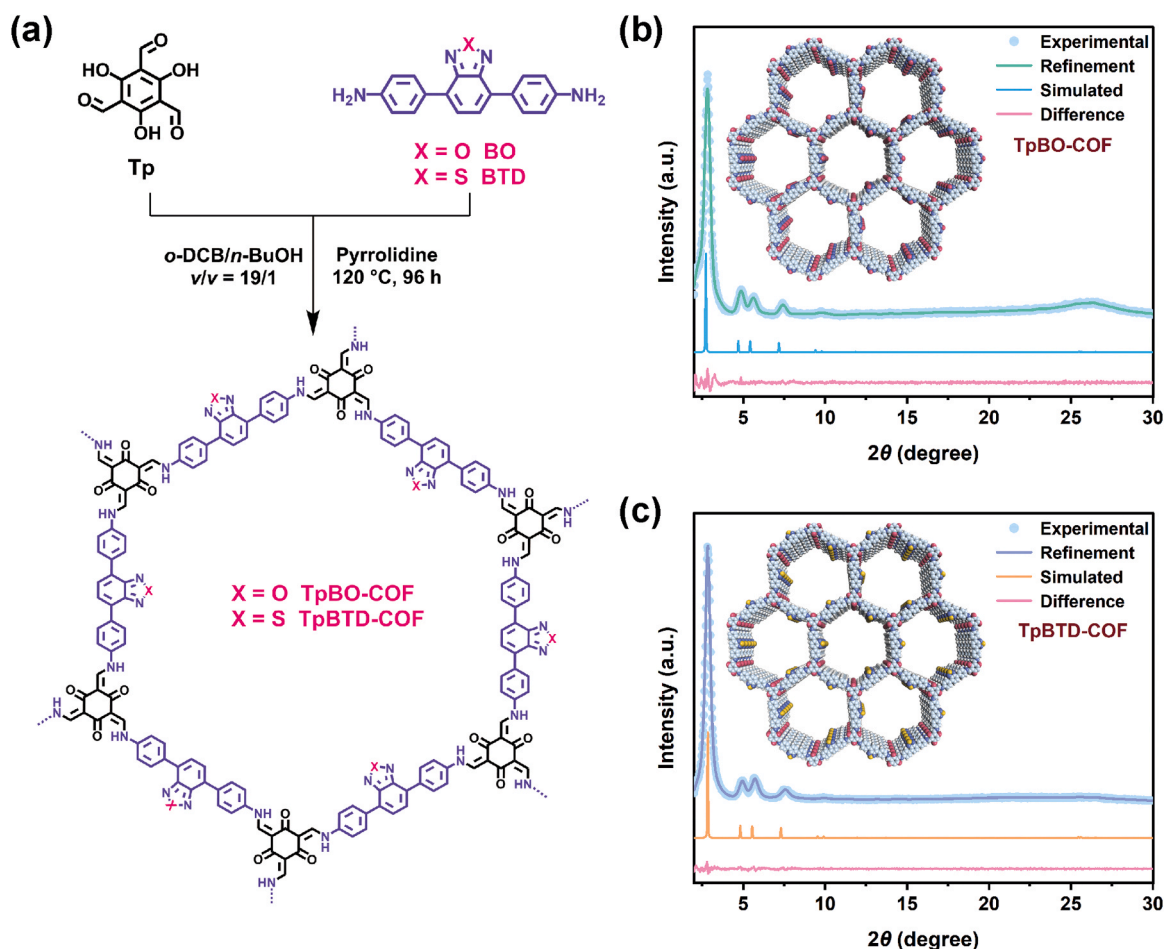*E-mail address:* xianjunlang@whu.edu.cn (X. Lang).

Fig. 1. (a) Syntheses of TpBO-COF and TpBTD-COF. Experimental and Pawley refined and simulated PXRD patterns, the top views of their AA stacking models of (b) TpBO-COF and (c) TpBTD-COF, respectively (O-atom: red, S-atom: orange, N-atom: purple, C-atom: light cyan, H-atom: white).

optoelectronic properties make them extensively explored in organic optoelectronic devices [52–54], due to the ease of preparation and the good stability of the underlying benzothiadiazole. Moreover, benzothiadiazole has also been incorporated into many COFs, showing excellent activity in water splitting and organic transformation [55–57], etc. In this vein, benzooxadiazole possesses a similar structure to benzothiadiazole by substituting the sulfur (S) atom with oxygen (O) atom [58]. Compared to benzothiadiazole, there are far fewer reports of benzooxadiazole as a building block for COFs. Benzooxadiazole demonstrates good electron-withdrawing ability due to the strong electron affinity of O-atom, which is beneficial for constructing COFs with low bandgaps and therefore wide visible light absorptions [59–61]. Given the intrinsic characteristics of benzooxadiazole and benzothiadiazole, inserting them into the skeletons of COFs can achieve precise heteroatom substitution to explore the impact of atomic changes on photocatalytic activity.

Herein, two building blocks of 4,4′-(benzooxadiazole-4,7-diyl)dianiline (BO) and 4,4′-(benzothiadiazole-4,7-diyl)dianiline (BTD) are synthesized for further condensations with 1,3,5-triformylphloroglucinol (Tp) to obtain two β-ketoenamine-linked COFs, TpBO-COF and TpBTD-COF (Fig. 1a), respectively. A series of optical and photoelectrochemical characterizations demonstrate that TpBO-COF has augmented visible light absorption and accelerated charge separation and transport compared to TpBTD-COF. Photocatalytic oxygenation can generate various organic compounds or intermediates under mild conditions, presenting enormous potential in producing fine chemicals and pharmaceuticals [62,63]. Thus, the photocatalytic activity of both COFs is compared using the oxygenation of sulfides to sulfoxides with

dioxygen (O₂) as a model reaction. TpBO-COF exhibits higher conversions in oxygenation of sulfides than TpBTD-COF. More importantly, the oxygenation conversions over both TpBO-COF and TpBTD-COF are prominently promoted after introducing the redox mediator 2,2,6,6-tetramethylpiperidinooxy (TEMPO), and TpBO-COF still has higher photocatalytic activity than TpBTD-COF after adding catalytic amount of TEMPO. The results indicate that heteroatom substitution impacts the photocatalytic activity of COFs. Furthermore, a cooperative platform for the photocatalytic oxygenation of organic sulfides is established over TpBO-COF and TEMPO irradiated by blue light. This work provides a rational design of the building blocks by heteroatom substitution in COFs to boost visible light photocatalytic activity.

2. Experimental section

2.1. Syntheses of TpBO-COF and TpBTD-COF

The syntheses of TpBO-COF and TpBTD-COF were conducted using pyrrolidine as the catalyst under solvothermal conditions. Specifically, Tp (10.5 mg, 0.05 mmol), BO (22.7 mg, 0.075 mmol) or BTD (23.9 mg, 0.075 mmol) were put into a 10 mL Pyrex tube. Upon addition of o-dichlorobenzene (o-DCB, 950 μL) and n-butanol (n-BuOH, 50 μL), the mixture was sonicated for 5 min. Then, pyrrolidine (20 μL) as the catalyst was added to the Pyrex tube along with ultrasonication again for 1 min. Subsequently, under 77 K nitrogen (N₂), the tube was frozen, degassed, and sealed with high-temperature flame. After heating for 96 h at 120 °C, the product was collected and rinsed with tetrahydrofuran (THF, 4 × 5 mL) and methanol (CH₃OH, 4 × 5 mL), followed by
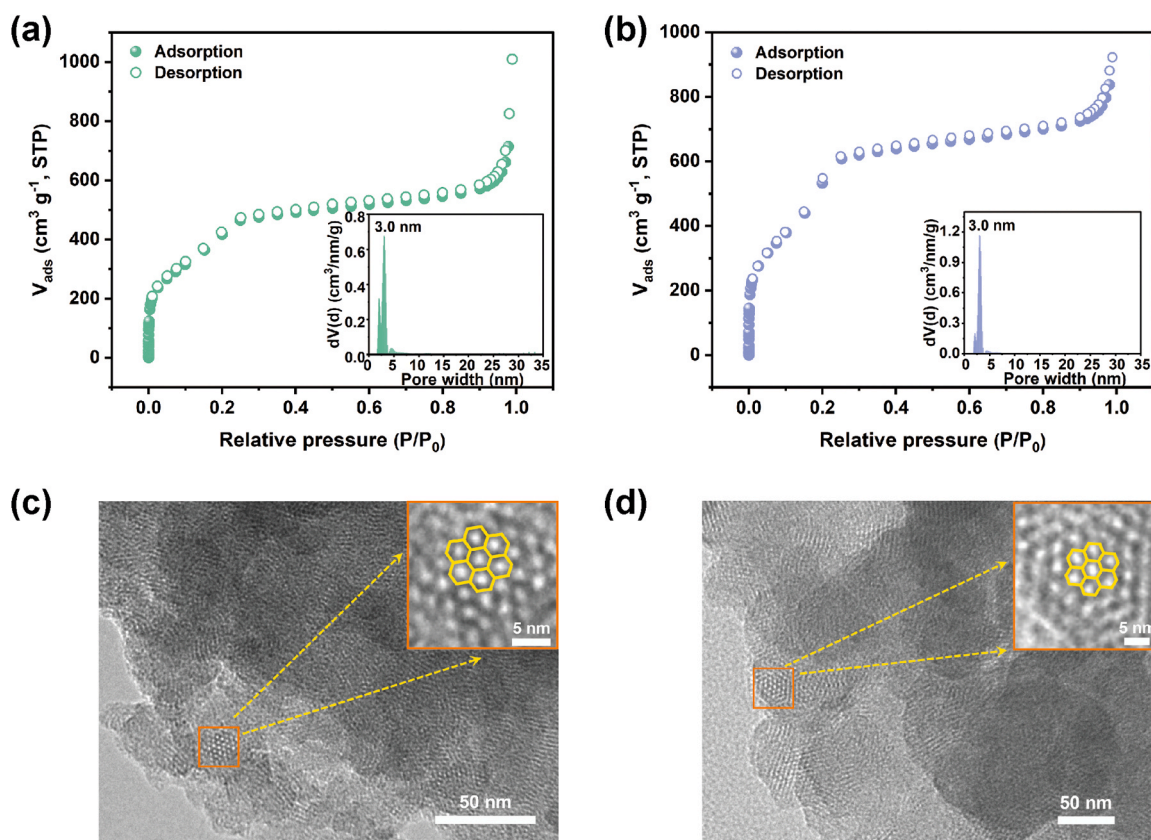
Fig. 2. N_2 adsorption and desorption isotherms at 77 K and pore-size distributions of (a) TpBO-COF, and (b) TpBTD-COF. TEM images of (c) TpBO-COF, and (d) TpBTD-COF.

Soxhlet extraction with THF for 48 h. After drying for 12 h at 80 °C, TpBO-COF and TpBTD-COF were obtained with yields of 79% and 82%, respectively.

2.2. General procedure of photocatalytic oxygenation of sulfide

In detail, COF photocatalyst (5 mg), organic sulfide (0.3 mmol) and TEMPO (9 μmol) were put into a Pyrex reactor (10 mL) and dispersed by CH_3OH (1 mL). Stirring for 15 min to achieve the adsorption–desorption equilibrium. Subsequently, the Pyrex reactor was filled with O_2 and irradiated by 460 nm blue light-emitting diodes (LEDs) for photocatalytic oxygenation. Analysis and detection of the target sulfoxide products were conducted using gas chromatography with a flame ionization detector (GC–FID) after the reaction with an internal standard of bromobenzene.

3. Result and discussion

3.1. Syntheses and characterizations of TpBO-COF and TpBTD-COF

The syntheses of TpBO-COF and TpBTD-COF were conducted by the condensation of Tp with BO and BTD, respectively, with pyrrolidine as the catalyst under solvothermal conditions (Fig. 1a). Firstly, the powder X-ray diffraction (PXRD) patterns showed intense diffractions of the predominant peaks, revealing the high crystallinity of TpBO-COF and TpBTD-COF (Fig. 1b and Fig. 1c). The six prominent diffraction peaks of TpBO-COF were situated at 2.8°, 4.9°, 5.6°, 7.4°, 9.8° and 25.8°, which correspond to the (100), (110), (200), (210), (220) and (001) lattice facets (Fig. S1a), respectively. Analogously, the PXRD pattern of TpBTD-COF also showed almost identical diffraction peak positions and lattice facets (Fig. S2a).

To determine the stackings of TpBO-COF and TpBTD-COF, their eclipsed (AA) and staggered (AB) stacking models were constructed. As shown in Fig. S1, TpBO-COF adopted the AA stacking, because the experimental PXRD pattern essentially matches the simulated AA-stacking PXRD pattern. In contrast, the simulated AB stacking pattern presented a large offset with the experimental PXRD pattern. By the same token, TpBTD-COF also followed the AA stacking by comparing the experimental with the simulated PXRD patterns (Fig. S2). Furthermore, by comparing the PXRD patterns of both COFs and their building blocks, it is shown that the building blocks formed the frameworks by condensation. Notably, both TpBO-COF and TpBTD-COF had good phase purity (Fig. S3).

The permanent porosity of TpBO-COF and TpBTD-COF was appraised by N_2 sorption measurements at 77 K (Fig. 2a and Fig. 2b). Both TpBO-COF and TpBTD-COF presented typical type-IV adsorption–desorption isotherms, reflecting their mesoporous characteristics. The Brunauer–Emmett–Teller (BET) specific surface areas of TpBO-COF and TpBTD-COF were 1108 and 1350 m^2 g^{-1}, respectively. Furthermore, depending on the nonlocal density functional theory (NLDFT) method, the calculated pore sizes of both TpBO-COF and TpBTD-COF were mainly distributed at 3.0 nm. Scanning electron microscopy (SEM) and transmission electron microscopy (TEM) were operated to assess the microscopic morphology and pore characteristics of both TpBO-COF and TpBTD-COF (Fig. S4). SEM images showed that TpBO-COF had a branched morphology of irregular particle aggregation, and TpBTD-COF exhibited a strip-shaped morphology composed of spheres. The high crystallinity and ordered hexagonal pore structure of both TpBO-COF and TpBTD-COF were further confirmed by TEM images (Fig. 2c and Fig. 2d).

The chemical structures of TpBO-COF and TpBTD-COF were identified by Fourier transform infrared (FTIR) spectroscopy. The FTIR spectra in Fig. S5a and Fig. S5b clearly showed the disappearance of $-NH_2$ characteristic signals (3300−3500 cm^{-1}) of both TpBO-COF and
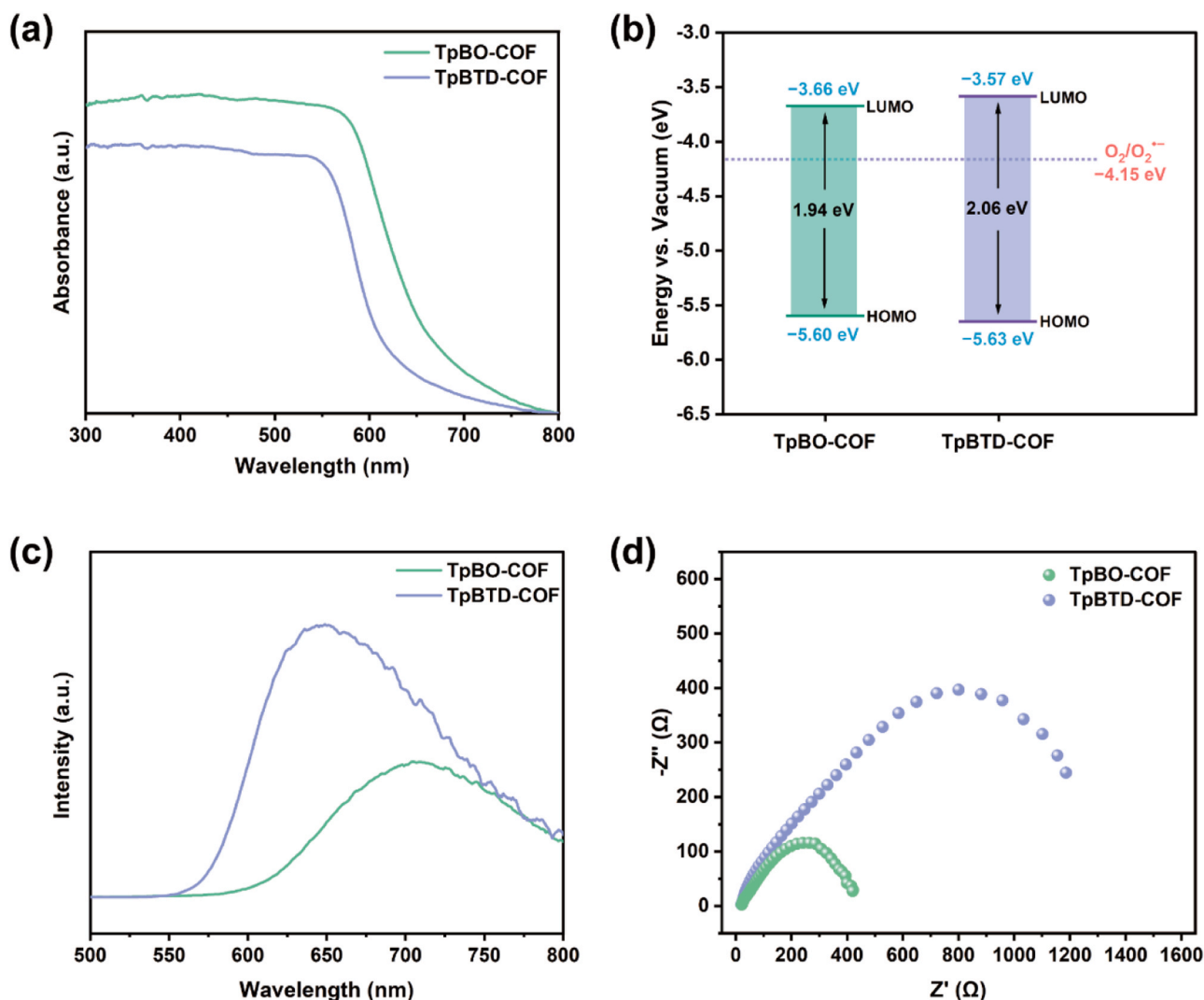
Fig. 3. (a) UV–visible DRS of TpBO-COF and TpBTD-COF. (b) Band positions of TpBO-COF and TpBTD-COF. (c) PL spectra of TpBO-COF and TpBTD–COF. (d) EIS Nyquist plots of TpBO-COF and TpBTD-COF.
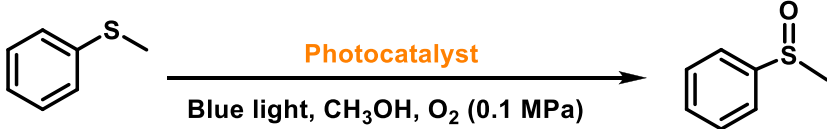
TpBTD-COF. Simultaneously, the emerged C=O stretching signals (~1621 cm^{-1}) and C−N characteristic signals (~1256 cm^{-1}) intuitively reflected the tautomerization of enol to keto [64,65]. The structural compositions of TpBO-COF and TpBTD-COF were further confirmed by solid-state ^{13}C nuclear magnetic resonance (NMR) spectroscopy (Fig. S5c and Fig. S5d). The characteristic signals of the carbon (C−N) at ~148 ppm and the carbonyl carbon (C=O) at ~185 ppm further supported the formation of the β-ketoenamine linkage [66]. FTIR and ^{13}C solid-state NMR mutually confirmed the establishment of two β-ketoenamine-linked COFs, TpBO-COF and TpBTD-COF, from their building blocks of Tp with BO and BTD, respectively. Besides, thermogravimetric analysis under an N$_2$ atmosphere revealed that both COFs were thermally stable up to ~400 °C (Fig. S6).

After confirming the successful syntheses of TpBO-COF and TpBTD-COF by the above characterizations, the light absorption capacity and band structures of TpBO-COF and TpBTD-COF were investigated and evaluated. As measured by UV–visible diffuse reflectance spectroscopy (DRS), both TpBO-COF and TpBTD-COF exhibited broad absorption in the visible light region (Fig. 3a). However, TpBO-COF showed augmented absorption compared to TpBTD-COF over the wavelength range of 550–800 nm. The optical bandgaps (E_g) of TpBO-COF and TpBTD-COF calculated from the Tauc plots were 1.94 and 2.06 eV (Fig. S7a), respectively. The LUMO levels of both TpBO-COF and TpBTD-

COF were estimated by electrochemical cyclic voltammetry (CV), and their CV curves were shown in Fig. S7b. The onset reduction potentials of TpBO-COF and TpBTD-COF were determined to be −0.70 and −0.79 V (vs. Ag/AgCl). According to the equation $E_{LUMO} = -[E_{red-onset} - E_{Fc/Fc+} + 4.8]$ eV [67,68], the E_{LUMO} values of TpBO-COF and TpBTD-COF were calculated to be −3.66 and −3.57 eV (vs. vacuum). Combining the values of E_g and E_{LUMO}, the E_{HOMO} values were also obtained and the corresponding band alignments were presented in Fig. 3b. From the energy level positions of TpBO-COF and TpBTD-COF, it can be inferred that the reduction of O$_2$ to O$_2^{2-}$ irradiated by visible light is highly plausible [69], which makes them ready for photocatalytic selective oxygenation.

Subsequently, the separation and transport of photogenerated electron–hole (e$^-$–h$^+$) pairs over TpBO-COF and TpBTD-COF were investigated. When excited at 375 nm, photoluminescence (PL) spectra of TpBO-COF and TpBTD-COF were gathered. TpBO-COF presented a lower PL intensity than TpBTD-COF (Fig. 3c). The recorded PL decay curves of TpBO-COF and TpBTD-COF were shown in Fig. S8. The average PL lifetimes of TpBO-COF and TpBTD-COF were 0.83 and 0.61 ns, respectively. Compared with TpBTD-COF, the reduced PL intensity and the extended PL lifetime of TpBO-COF indicated the slower recombination of photogenerated charge carriers in TpBO-COF. Additionally, TpBO-COF possessed an enhanced photocurrent intensity than

Table 1
The comparison of photocatalytic oxygenation of methyl phenyl sulfide over TpBO-COF and TpBTD-COF[a].

Entry	Photocatalyst	TEMPO (%)	Conv. (%)[b]	Sel. (%)[b]
1	TpBO-COF	0	36	99
2	TpBTD-COF	0	19	99
3	TpBO-COF	3	82	97
4	TpBTD-COF	3	61	98
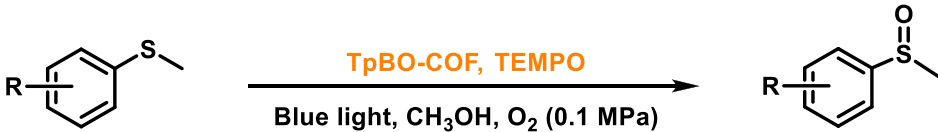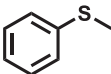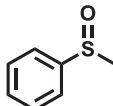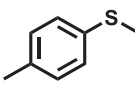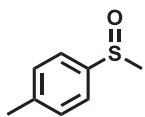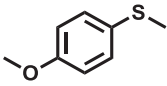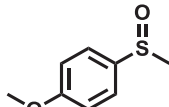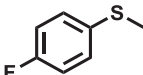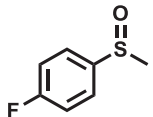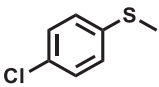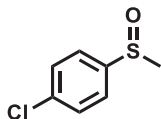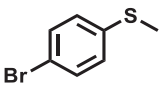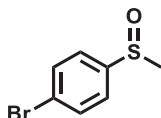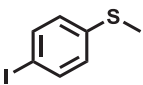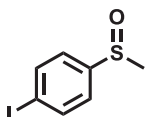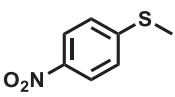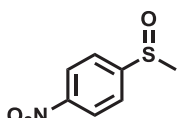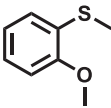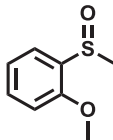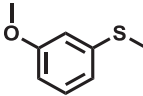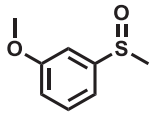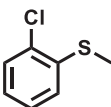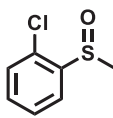
[a] Reaction conditions: COF (5 mg), methyl phenyl sulfide (0.3 mmol), CH_3OH (1 mL), blue LEDs (460 ± 10 nm, 3 W × 4), O_2 (0.1 MPa), 1.5 h.

[b] Conversion of sulfide and selectivity of sulfoxide were determined by GC–FID.
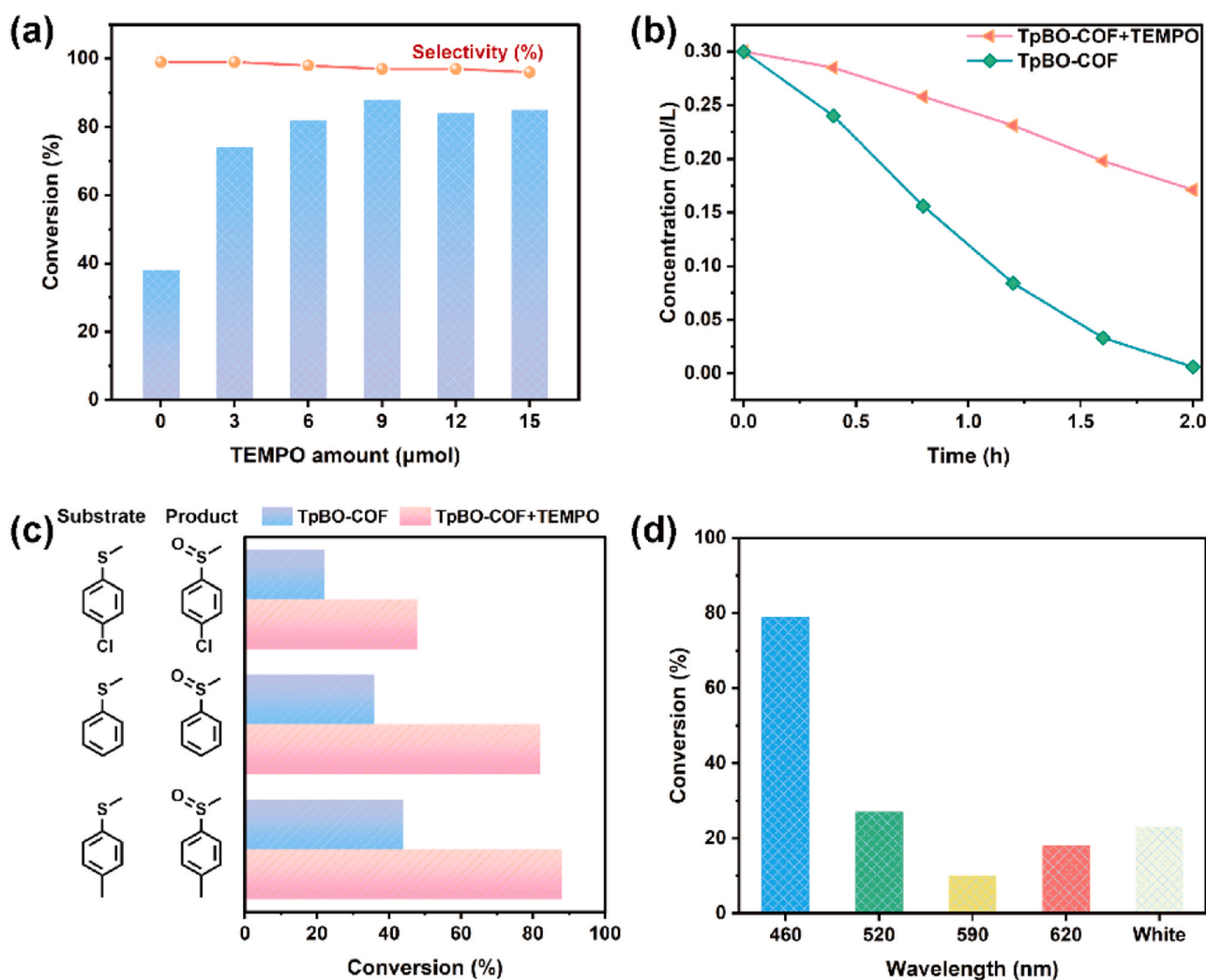
Fig. 4. (a) The effect of different amounts of TEMPO on photocatalytic oxygenation of methyl phenyl sulfide over TpBO-COF. (b) Kinetic studies of reaction process for photocatalytic oxygenation of methyl phenyl sulfide over TpBO-COF with or without 3% of TEMPO. (c) Comparison of photocatalytic oxygenation of three methyl phenyl sulfides with different substituents. (d) The influence of LEDs with different peak wavelengths on the photocatalytic oxygenation of methyl phenyl sulfide. Reaction conditions: TpBO-COF (5 mg), organic sulfide (0.3 mmol), O_2 (0.1 MPa), LEDs (3 W × 4), CH_3OH (1 mL). Reaction time: (a) 1.8 h; (c) and (d) 1.5 h.

TpBTD-COF in the on/off cycle of light (Fig. S7d), manifesting a more effective charge separation capacity of TpBO-COF. Electrochemical impedance spectroscopy (EIS) Nyquist plots showcased a smaller semicircular radius of TpBO-COF than that of TpBTD-COF (Fig. 3d), demonstrating the lower charge migration resistance of TpBO-COF. Based on the above characterizations, heteroatom substitution in the structure of COF can improve charge separation and transport efficiency.
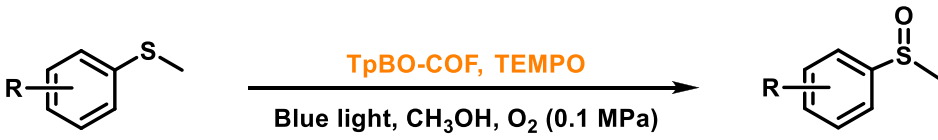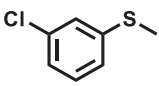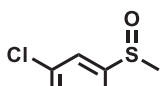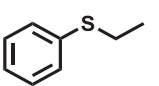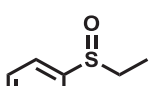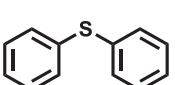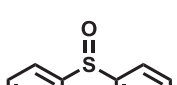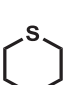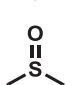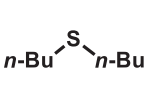
Table 2

Scope for the photocatalytic oxygenation of organic sulfides with O_2 over TpBO-COF and TEMPO[a].

Entry	Substrate	Product	Conv. (%)[b]	Sel. (%)[b]
1			93	97
2			99	97
3			98	97
4			85	95
5			75	96
6			79	94
7			86	95
8			8	78
9			96	99
10			92	97
11			25	98

Table 2 (*continued*)

Entry	Substrate	Product	Conv. (%)[b]	Sel. (%)[b]
12			48	95
13			78	86
14			2	99
15[c]			93	98
16[c]			99	96

[a] Reaction conditions: TpBO-COF (5 mg), sulfide (0.3 mmol), O$_2$ (0.1 MPa), blue LEDs (460 ± 10 nm, 3 W × 4), CH$_3$OH (1 mL), 2.0 h.
[b] Conversion and selectivity detected by GC–FID using bromobenzene as the internal standard.
[c] 1.0 h.

3.2. Photocatalytic oxygenation of sulfides over TpBO-COF and TpBTD-COF

As important bioactive compounds, organic sulfoxides are generally used in the synthesis and development of pharmaceuticals, agrochemicals, and fine chemicals. The photocatalytic generation of organic sulfoxides is promising because of its cleanness and high selectivity [70–73]. Superoxide anion radical (O$_2^{\bullet-}$) usually plays a prominent role in photocatalytic oxygenation of sulfides. In view of the appropriate energy band positions for the generation of O$_2^{\bullet-}$, both TpBO-COF and TpBTD-COF were used as the photocatalysts for the oxygenation of sulfides to evaluate their activity. As shown in Table 1, both TpBO-COF and TpBTD-COF achieved the oxygenation of methyl phenyl sulfide irradiated by blue LEDs. However, TpBO-COF presented a higher conversion of methyl phenyl sulfide than TpBTD-COF (Table 1, entries 1 and 2), suggesting the heteroatom substitution of COFs could improve the photocatalytic activity. Subsequently, a catalytic amount of TEMPO was introduced to determine whether it had a promoting effect with TpBO-COF and TpBTD-COF. As a result, both TpBO-COF and TpBTD-COF acquired significant improvements in the conversion of methyl phenyl sulfide with 3% of TEMPO. Due to the faster charge separation and transport, the conversion of methyl phenyl sulfide over TpBO-COF was still higher than that of TpBTD-COF with 3% of TEMPO under the same reaction conditions (Table 1, entries 3 and 4).

Considering the superiority of TpBO-COF over TpBTD-COF, TpBO-COF was used to comprehensively investigate the photocatalytic oxygenation of sulfides with TEMPO. TEMPO acts as an h$^+$ transfer mediator, and an appropriate amount of TEMPO can optimize the efficiency. Thus, investigations of the effect of different amounts (0–5%) of TEMPO were conducted on the oxygenation of methyl phenyl sulfide (Fig. 4a). When 3% of TEMPO was added, the optimal conversion was

obtained. In subsequent experiments, 3% of TEMPO was opted to promote the reaction progress. Kinetic studies further revealed that TEMPO eminently accelerates the oxygenation of methyl phenyl sulfide throughout the entire reaction progress (Fig. 4b). Moreover, to determine the applicability of the promoting effect of TEMPO, three methyl phenyl sulfides with different substituents were selected to conduct the photocatalytic test (Fig. 4c). With the addition of 3% of TEMPO, the conversions of three sulfides over TpBO-COF were more than twice of that without TEMPO. The electrical power was precisely controlled at 3 W × 4 for LEDs. However, there might be different photoelectric conversion efficiencies and therefore the comparison should be only conclusive for the LEDs but cannot be compelling for the wavelength. Thus, LEDs with different peak wavelengths were used for photocatalytic oxygenation (Fig. 4d). Specifically, TpBO-COF presented moderate activity of the photocatalytic oxygenation of methyl phenyl sulfide irradiated by 520, 590, 620 nm LEDs and white LEDs. The most efficient conversion was achieved irradiated by 460 nm blue LEDs. Photocatalytic activity tests were also conducted over the building blocks of Tp, BO, and BTD with or without TEMPO. The photocatalytic activities of Tp and BO were much lower than TpBO-COF with TEMPO in particular (Table S1, entries 1–6). Additionally, when 3% of TEMPO$^+$BF$_4^-$ (2,2,6,6-tetramethylpiperidine-1-oxoammonium tetrafluoroborate) was added instead of 3% of TEMPO, 59% conversion was obtained within 1.5 h. The salt of TEMPO like TEMPO$^+$BF$_4^-$ can be an h$^+$ transfer mediator, but the promoting effect with TpBO-COF is less pronounced.

To further examine the generality and the scope, a series of organic sulfides were used to conduct the photocatalytic oxygenation with O$_2$ over TpBO-COF and TEMPO (Table 2). On the whole, all sulfide substrates could be transformed into the corresponding sulfoxides in varying degrees. In detail, for methyl phenyl sulfides, those have *para*
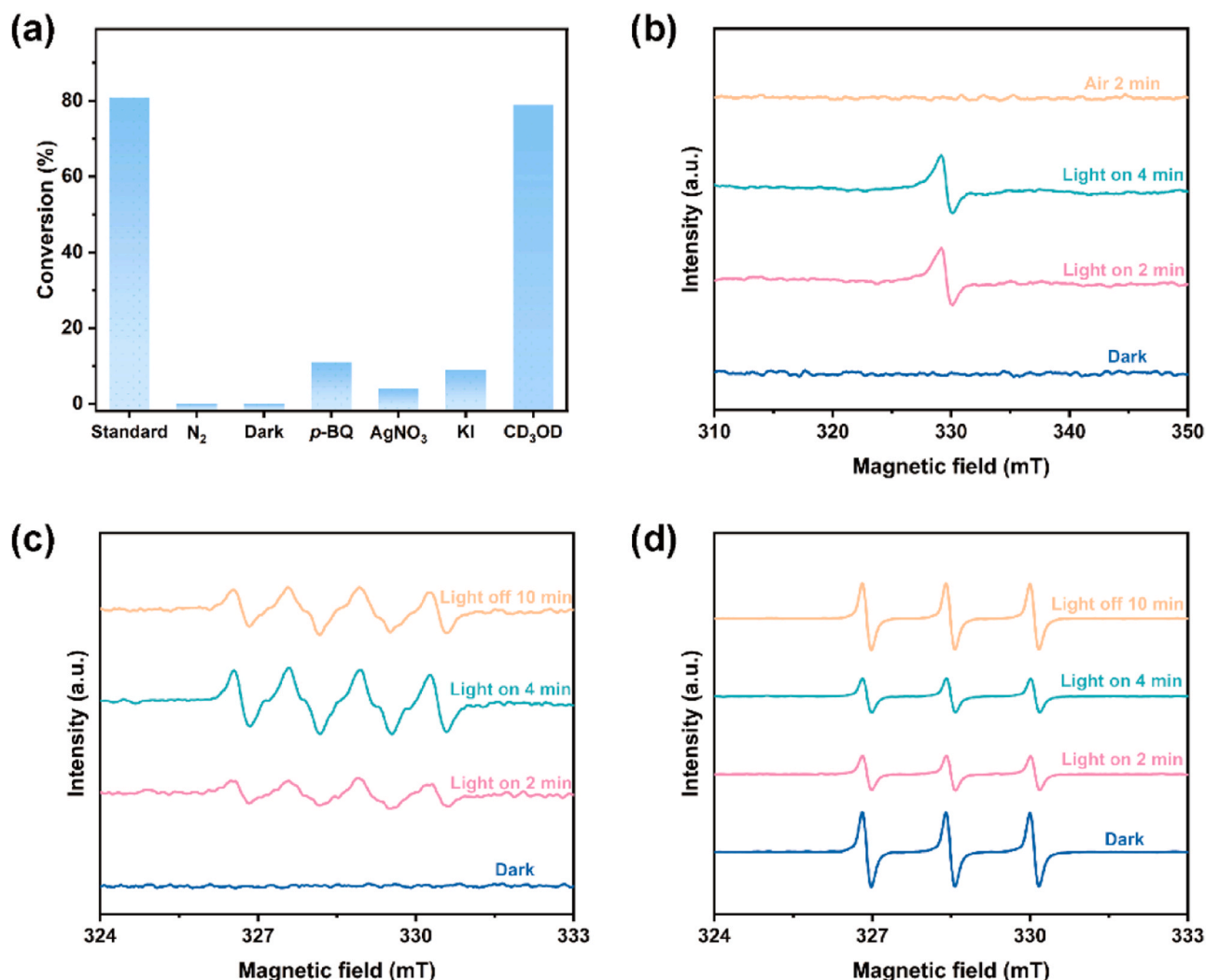
Fig. 5. (a) Control and quenching tests for oxygenation of methyl phenyl sulfide over TpBO-COF, standard reaction conditions: TpBO-COF (5 mg), methyl phenyl sulfide (0.3 mmol), O_2 (0.1 MPa), blue LEDs (460 ± 10 nm, 3 W × 4), CH_3OH (1 mL), 1.5 h. Detected EPR signals of (b) e^-, (c) DMPO captured $O_2^{\bullet-}$, (d) TEMPO.

electron-donating substituents, the conversions were generally higher than those with *para* electron-withdrawing substituents (Table 2, entries 1–8). The positions of the substituent on the phenyl ring affected the photocatalytic activity of TpBO-COF and TEMPO. For $-OCH_3$ with the electron-donating substitution, the order presented of conversions was p-OCH_3 > o-OCH_3 > m-OCH_3 (Table 2, entries 3, 9 and 10), and the conversion order was p-Cl > m-Cl > o-Cl for $-$Cl with electron-withdrawing substitution (Table 2, entries 5, 11 and 12). The conversion decreased when the methyl group of methyl phenyl sulfide was replaced with an ethyl group, and the conversion dropped dramatically when replaced with a phenyl group (Table 2, entry 1 vs. enteries 13 and 14), indicating that the steric hindrance of substituents significantly affects the photocatalytic activity. Moreover, aliphatic sulfides such as pentamethylene sulfide and di-*tert* butyl (n-Bu) sulfide completed over 90% conversions within 1 h (Table 2, entries 15 and 16). Then, cycling stability tests of of TpBO-COF were conducted using methyl phenyl sulfide as the substrate. In all five cycles, this photocatalytic system maintained high conversions above 90% (Fig. S9a), and FTIR and UV-visible DRS after the reaction displayed no significant differences compared to the TpBO-COF before reaction (Fig. S9b and Fig. S9c). Besides, the morphology of TpBO-COF was not notably damaged either (Fig. S9d), showcasing the good stability of photocatalytic activity and chemical structure.

3.3. Mechanistic studies of photocatalytic oxygenation over TpBO-COF

After verifying the superiority, mechanistic studies were conducted for photocatalytic oxygenation of sulfides over TpBO-COF and TEMPO. Ordinarily, the oxidant for photocatalytic selective oxygenation is O_2. As shown in Fig. 5a, the reaction didn't occur when replacing O_2 with N_2. Similarly, the reaction didn't happen when turning off the blue LEDs. Both results indicated the critical roles of both O_2 and blue light in the oxygenation. Then, 0.2 equivalent of p-benzoquinone (p-BQ) was added to the reaction system to capture $O_2^{\bullet-}$ generated in the reaction progress, only 11% conversion was obtained. It suggests that $O_2^{\bullet-}$ was vitally involved in the oxygenation of methyl phenyl sulfide. Next, 1 equivalent of silver nitrate ($AgNO_3$) and 1 equivalent of potassium iodide (KI) were employed as e^- scavenger and h^+ scavenger, respectively, the conversions of methyl phenyl sulfide sharply decreased, indicating that electron transfer pathway is essential to the oxygenation of methyl phenyl sulfide. Generally, the lifetime of singlet oxygen ($^1O_2$) could be prolonged by deuterated solvents [74]. So CD_3OD solvent was adopted to prolong the lifetime of $^1O_2$ in the control experiment. The conversion didn't show any obvious increase than that of CH_3OH as the solvent, indicating that $^1O_2$ does not play a prominent role in the oxygenation of methyl phenyl sulfide over TpBO-COF and TEMPO.

Meanwhile, electron paramagnetic resonance (EPR) spectroscopy was used to monitor the photogenerated e^-, $O_2^{\bullet-}$, and TEMPO signals in
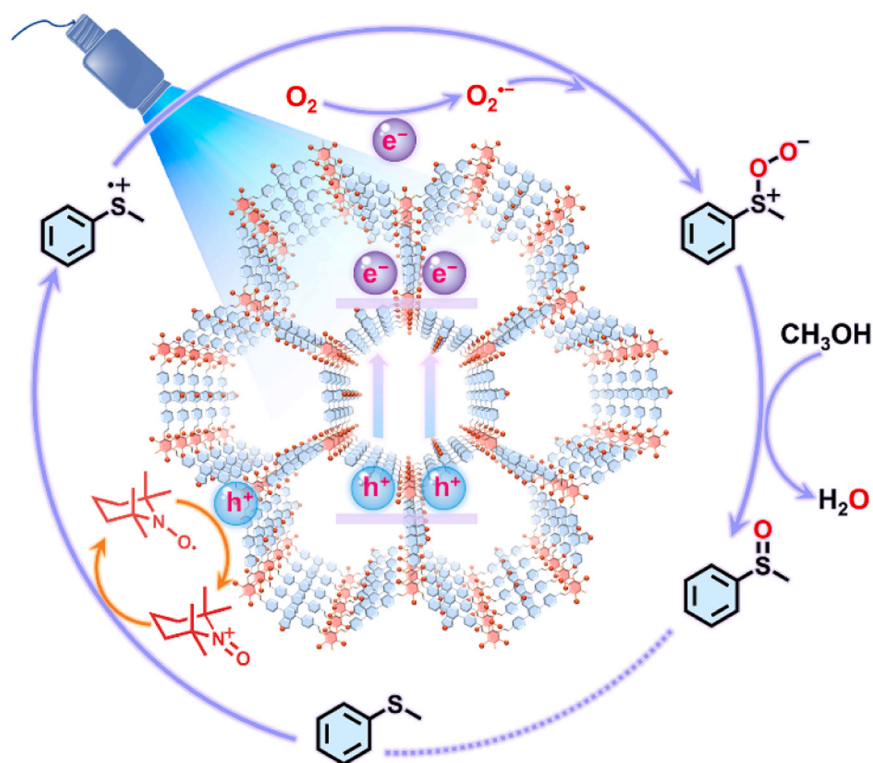
Fig. 6. A conceivable mechanism for photocatalytic oxygenation of methyl phenyl sulfide with O_2 over TpBO-COF and TEMPO.

the reaction progress. The signals of e^- were getting stronger irradiated by visible light, indicating charge separation happened on TpBO-COF (Fig. 5b). 5,5-Dimethyl-1-pyrroline *N*-oxide (DMPO) is frequently used to capture the $O_2^{\bullet-}$ and the DMPO-$O_2^{\bullet-}$ adduct was detected by EPR. As indicated in Fig. 5c, the signals of DMPO-$O_2^{\bullet-}$ were remarkably enhanced irradiated by visible light. The EPR results displayed that photogenerated e^- were used to activate O_2 to $O_2^{\bullet-}$. As a common and stable free radical, TEMPO can also be straightly detected through EPR. In the dark, the TEMPO signals measured were intense (Fig. 5d). The TEMPO signals continuously decayed irradiated by visible light. Furthermore, the TEMPO signals gradually recovered after removing the light. The results of TEMPO signals indicated that there existed a reversible alternation of TEMPO and TEMPO$^+$.

Combining the EPR results, control and quenching experiments, a conceivable mechanism for photocatalytic oxygenation of methyl phenyl sulfide over TpBO-COF and TEMPO is presented in Fig. 6. Irradiated by blue LEDs, e^- and h^+ generated by photoexcitation separate and transfer over TpBO-COF. Subsequently, e^- and h^+ propel the reduction of O_2 to $O_2^{\bullet-}$ and the oxidation of TEMPO to TEMPO$^+$, respectively. The formed TEMPO$^+$ promotes the conversion of methyl phenyl sulfide to sulfur radical cation, returning back to TEMPO. Then, the sulfur radical cation is attacked by $O_2^{\bullet-}$ to obtain the peroxysulfoxide intermediate. Finally, the target sulfoxide is obtained from the conversion of the peroxysulfoxide intermediate with the participation of CH_3OH. Importantly, the reversible alternation of TEMPO to TEMPO$^+$ promotes the h^+ transfer, exerting a promoting effect on the reaction conversion.

4. Conclusions

To sum up, two COFs, TpBO-COF and TpBTD-COF with different but precise heteroatom substitution (O and S) have been synthesized by rational design of building blocks, which both exhibited high crystallinity and excellent porosity. Compared with TpBTD-COF, TpBO-COF showed an augmented visible light harvesting region and accelerated charge separation and transport efficiency. TpBO-COF displayed faster conversions of the photocatalytic oxygenation of sulfides than TpBTD-COF. More importantly, the conversions dramatically increased with the addition of a catalytic amount of TEMPO. Additionally, the conceivable mechanism of efficient photocatalytic oxygenation of sulfides over TpBO-COF and TEMPO was concluded. Compellingly, a cooperative platform over the highly crystalline TpBO-COF was established with TEMPO for the photocatalytic oxygenation of organic sulfides to corresponding sulfoxides with O_2. This work offers a strategy of tuning photocatalytic activity by rational design of the building blocks with precise heteroatom substitution for COFs.

CRediT authorship contribution statement

Hongxiang Zhao: Writing – original draft, Investigation, Formal analysis. **Yuexin Wang:** Investigation, Formal analysis. **Fulin Zhang:** Investigation, Formal analysis. **Xiaoyun Dong:** Investigation, Formal analysis. **Xianjun Lang:** Writing – review & editing, Supervision, Conceptualization.

Declaration of Competing Interest

The authors declare that they have no known competing financial interests or personal relationships that could have appeared to influence the work reported in this paper.

Data Availability

Data will be made available on request.

Acknowledgments

Microscopy at Wuhan University for materials characterizations.

Appendix A. Supporting information

Supplementary data associated with this article can be found in the online version at doi:10.1016/j.apcatb.2024.123899.

References

[1] Y.O. Wang, A. Vogel, M. Sachs, R.S. Sprick, L. Wilbraham, S.J.A. Moniz, R. Godin, M.A. Zwijnenburg, J.R. Durrant, A.I. Cooper, J.W. Tang, Current understanding and challenges of solar-driven hydrogen generation using polymeric photocatalysts, Nat. Energy 4 (2019) 746–760, https://doi.org/10.1038/s41560-019-0456-5.

[2] X.D. Sun, S.Y. Jiang, H.W. Huang, H. Li, B.H. Jia, T.Y. Ma, Solar energy catalysis, Angew. Chem. Int. Ed. 61 (2022) e202204880, https://doi.org/10.1002/anie.202204880.

[3] H.L. Wu, M.Y. Qi, Z.R. Tang, Y.J. Xu, Semiconductor quantum dots: A versatile platform for photoredox organic transformation, J. Mater. Chem. A 11 (2023) 3262–3280, https://doi.org/10.1039/d2ta09423a.

[4] R.C. Shen, G.J. Liang, L. Hao, P. Zhang, X. Li, In-situ synthesis of chemically bonded 2D/2D covalent organic frameworks/O-vacancy WO₃ Z-scheme heterostructure for photocatalytic overall water splitting, Adv. Mater. 35 (2023) 2303649, https://doi.org/10.1002/adma.202303649.

[5] Y. Yang, X.Y. Chu, H.Y. Zhang, R. Zhang, Y.H. Liu, F.M. Zhang, M. Lu, Z.D. Yang, Y. Q. Lan, Engineering β-ketoamine covalent organic frameworks for photocatalytic overall water splitting, Nat. Commun. 14 (2023) 593, https://doi.org/10.1038/s41467-023-36338-x.

[6] Z.F. Zhao, X.P. Chen, B.Y. Li, S. Zhao, L.W. Niu, Z.J. Zhang, Y. Chen, Spatial regulation of acceptor units in olefin-linked COFs toward highly efficient photocatalytic H₂ evolution, Adv. Sci. 9 (2022) 2203832, https://doi.org/10.1002/advs.202203832.

[7] K. Kamada, J. Jung, T. Wakabayashi, K. Sekizawa, S. Sato, T. Morikawa, S. Fukuzumi, S. Saito, Photocatalytic CO₂ reduction using a robust multifunctional iridium complex toward the selective formation of formic acid, J. Am. Chem. Soc. 142 (2020) 10261–10266, https://doi.org/10.1021/jacs.0c03097.

[8] K. Sun, Y.Y. Qian, H.L. Jiang, Metal-organic frameworks for photocatalytic water splitting and CO₂ reduction, Angew. Chem. Int. Ed. 62 (2023) e202217565, https://doi.org/10.1002/anie.202217565.

[9] Q. Li, J. Wang, Y.Z. Zhang, L. Ricardez-Sandoval, G.Y. Bai, X.W. Lan, Structural and morphological engineering of benzothiadiazole-based covalent organic frameworks for visible light-driven oxidative coupling of amines, ACS Appl. Mater. Interfaces 13 (2021) 39291–39303, https://doi.org/10.1021/acsami.1c08951.

[10] H. Chen, H.S. Jena, X. Feng, K. Leus, P. Van der Voort, Engineering covalent organic frameworks as heterogeneous photocatalysts for organic transformations, Angew. Chem. Int. Ed. 61 (2022) e202204938, https://doi.org/10.1002/anie.202204938.

[11] Q. Yang, M.L. Luo, K.W. Liu, H.M. Cao, H.J. Yan, Covalent organic frameworks for photocatalytic applications, Appl. Catal. B 276 (2020) 119174, https://doi.org/10.1016/j.apcatb.2020.119174.

[12] H.J. Yang, R. Zhao, J.F. Wang, X.Y. Yin, Z. Lu, L.X. Hou, Local electron donor defects induce dipole polarization boosting on covalent organic frameworks to promote photocatalysis, ACS Mater. Lett. 5 (2023) 2877–2886, https://doi.org/10.1021/acsmaterialslett.3c01007.

[13] F.N. Hao, C. Yang, X.M. Lv, F.S. Chen, S.Y. Wang, G.F. Zheng, Q. Han, Photo-driven quasi-topological transformation exposing highly active nitrogen cation sites for enhanced photocatalytic H₂O₂ production, Angew. Chem. Int. Ed. 62 (2023) e202315456, https://doi.org/10.1002/anie.202315456.

[14] C.Z. Han, P.H. Dong, H.R. Tang, P.Y. Zheng, C. Zhang, F. Wang, F. Huang, J. X. Jiang, Realizing high hydrogen evolution activity under visible light using narrow band gap organic photocatalysts, Chem. Sci. 12 (2021) 1796–1802, https://doi.org/10.1039/d0sc05866a.

[15] K. Wu, X.Y. Liu, M. Xie, P.W. Cheng, J. Zheng, W.G. Lu, D. Li, Rational design of D−π−A−π−D porous organic polymer with polarized π for photocatalytic aerobic oxidation, Appl. Catal. B 334 (2023) 122847, https://doi.org/10.1016/j.apcatb.2023.122847.

[16] C. Lin, Z. Shan, C.R. Dong, Y. Lu, W.K. Meng, G. Zhang, B. Cai, G.Y. Su, J.H. Park, K. Zhang, Covalent organic frameworks bearing Ni active sites for free radical-mediated photoelectrochemical organic transformations, Sci. Adv. 9 (2023) eadi9442, https://doi.org/10.1126/sciadv.adi9442.

[17] S.M. Chai, X.W. Chen, X.R. Zhang, Y.X. Fang, R.S. Sprick, X. Chen, Rational design of covalent organic frameworks for efficient photocatalytic hydrogen peroxide production, Environ. Sci.: Nano 9 (2022) 2464–2469, https://doi.org/10.1039/d2en00135g.

[18] Z.P. Xie, X.B. Yang, P. Zhang, X.T. Ke, X. Yuan, L.P. Zhai, W.B. Wang, N. Qin, C. X. Cui, L.B. Qu, X. Chen, Vinylene-linked covalent organic frameworks with manipulated electronic structures for efficient solar-driven photocatalytic hydrogen production, Chin. J. Catal. 47 (2023) 171–180, https://doi.org/10.1016/s1872-2067(23)64397-9.

[19] Z.P. Xie, W.B. Wang, X.T. Ke, X. Cai, X. Chen, S.B. Wang, W. Lin, X.C. Wang, A heptazine-based polymer photocatalyst with donor-acceptor configuration to promote exciton dissociation and charge separation, Appl. Catal. B 325 (2023) 122312, https://doi.org/10.1016/j.apcatb.2022.122312.

[20] Z.P. Luo, X.W. Chen, Y.Y. Hu, X. Chen, W. Lin, X.F. Wu, X.C. Wang, Side-chain molecular engineering of triazole-based donor-acceptor polymeric photocatalysts with strong electron push-pull interactions, Angew. Chem. Int. Ed. 62 (2023) e202304875, https://doi.org/10.1002/anie.202304875.

[21] S.D. Wang, Z.P. Xie, D. Zhu, S. Fu, Y.S. Wu, H.L. Yu, C.Y. Lu, P.K. Zhou, M. Bonn, H. I. Wang, Q. Liao, H. Xu, X. Chen, C. Gu, Efficient photocatalytic production of hydrogen peroxide using dispersible and photoactive porous polymers, Nat. Commun. 14 (2023) 6891, https://doi.org/10.1038/s41467-023-42720-6.

[22] S. Suleman, X.Y. Guan, Y. Zhang, A. Waseem, O. Metin, Z. Meng, H.L. Jiang, Regulating the generation of reactive oxygen species for photocatalytic oxidation by metalloporphyrinic covalent organic frameworks, Chem. Eng. J. 476 (2023) 146623, https://doi.org/10.1016/j.cej.2023.146623.

[23] W.K. Qin, C.H. Tung, L.Z. Wu, Covalent organic framework and hydrogen-bonded organic framework for solar-driven photocatalysis, J. Mater. Chem. A 11 (2023) 12521–12538, https://doi.org/10.1039/d2ta09375h.

[24] J.Z. Li, D.G. Ma, Q. Huang, Y.Y. Du, Q. He, H.W. Ji, W.H. Ma, J.C. Zhao, Cu²⁺ coordination-induced in situ photo-to-heat on catalytic sites to hydrolyze β-lactam antibiotics pollutants in waters, Proc. Natl. Acad. Sci. U. S. A. 120 (2023) e2302761120, https://doi.org/10.1073/pnas.2302761120.

[25] S. Ma, T.Q. Deng, Z.P. Li, Z.W. Zhang, J. Jia, G. Wu, H. Xia, S.W. Yang, X.M. Liu, Photocatalytic hydrogen production on a sp²-carbon-linked covalent organic framework, Angew. Chem. Int. Ed. 61 (2022) e202208919, https://doi.org/10.1002/anie.202208919.

[26] P.N. Shang, X.L. Yan, Y. Li, J.J. Liu, G. Zhang, L. Chen, Heterogeneous photocatalytic borylation of aryl iodides mediated by isoreticular 2D covalent organic frameworks, Chin. Chem. Lett. 34 (2023) 107584, https://doi.org/10.1016/j.cclet.2022.06.007.

[27] X.R. Chen, C.R. Zhang, X. Liu, R.P. Liang, J.D. Qiu, Ionic covalent organic framework for selective detection and adsorption of TcO₄⁻/ReO₄⁻, Chem. Commun. 59 (2023) 9521–9524, https://doi.org/10.1039/d3cc02429f.

[28] D. Chen, W.B. Chen, G. Zhang, S. Li, W.H. Chen, G.L. Xing, L. Chen, N-rich 2D heptazine covalent organic frameworks as efficient metal-free photocatalysts, ACS Catal. 12 (2022) 616–623, https://doi.org/10.1021/acscatal.1c05233.

[29] K.T. Tan, S. Ghosh, Z.Y. Wang, F.X. Wen, D. Rodríguez-San-Miguel, J. Feng, N. Huang, W. Wang, F. Zamora, X.L. Feng, A. Thomas, D.L. Jiang, Covalent organic frameworks, Nat. Rev. Methods Primers 3 (2023) 1, https://doi.org/10.1038/s43586-022-00181-z.

[30] S. Kandambeth, K. Dey, R. Banerjee, Covalent organic frameworks: Chemistry beyond the structure, J. Am. Chem. Soc. 141 (2019) 1807–1822, https://doi.org/10.1021/jacs.8b10334.

[31] X.W. Li, S. Yang, M.H. Liu, X.B. Yang, Q. Xu, G.F. Zeng, Z. Jiang, Catalytic linkage engineering of covalent organic frameworks for the oxygen reduction reaction, Angew. Chem. Int. Ed. (2023) e202304356, https://doi.org/10.1002/anie.202304356.

[32] Y. Su, B. Li, H. Xu, C.Y. Lu, S.D. Wang, B. Chen, Z.M. Wang, W.T. Wang, K. Otake, S. Kitagawa, L.B. Huang, C. Gu, Multi-component synthesis of a buta-1,3-diene-linked covalent organic framework, J. Am. Chem. Soc. 144 (2022) 18218–18222, https://doi.org/10.1021/jacs.2c05701.

[33] R.H. Xu, W.R. Cui, C.R. Zhang, X.R. Chen, W. Jiang, R.P. Liang, J.D. Qiu, Vinylene-linked covalent organic frameworks with enhanced uranium adsorption through three synergistic mechanisms, Chem. Eng. J. 419 (2021) 129550, https://doi.org/10.1016/j.cej.2021.129550.

[34] Z.J. Yong, T.Y. Ma, Solar-to-H₂O₂ catalyzed by covalent organic frameworks, Angew. Chem. Int. Ed. 62 (2023) e202308980, https://doi.org/10.1002/anie.202308980.

[35] K.R. Cai, W.J. Wang, J. Zhang, L. Chen, L.K. Wang, X.J. Zhu, Z.P. Yu, Z.C. Wu, H. P. Zhou, Facile construction of olefin-linked covalent organic frameworks for enhanced photocatalytic organic transformation via wall surface engineering, J. Mater. Chem. A 10 (2022) 7165–7172, https://doi.org/10.1039/d1ta09684b.

[36] F.L. Zhang, X. Li, X.Y. Dong, H.M. Hao, X.J. Lang, Thiazolo[5,4-d]thiazole-based covalent organic framework microspheres for blue light photocatalytic selective oxidation of amines with O₂, Chin. J. Catal. 43 (2022) 2395–2404, https://doi.org/10.1016/s1872-2067(22)64127-5.

[37] W. Zhao, P.Y. Yan, B.Y. Li, M. Bahri, L.J. Liu, X. Zhou, R. Clowes, N.D. Browning, Y. Wu, J.W. Ward, A.I. Cooper, Accelerated synthesis and discovery of covalent organic framework photocatalysts for hydrogen peroxide production, J. Am. Chem. Soc. 144 (2022) 9902–9909, https://doi.org/10.1021/jacs.2c02666.

[38] D.M. Tan, R. Zhuang, R.C. Chen, M.H. Ban, W. Feng, F. Xu, X. Chen, Q.Y. Wang, Covalent organic frameworks enable sustainable solar to hydrogen peroxide, Adv. Funct. Mater. (2023) 2311655, https://doi.org/10.1002/adfm.202311655.

[39] J. Xiao, X.L. Liu, L. Pan, C.X. Shi, X.W. Zhang, J.J. Zou, Heterogeneous photocatalytic organic transformation reactions using conjugated polymers-based materials, ACS Catal. 10 (2020) 12256–12283, https://doi.org/10.1021/acscatal.0c03480.

[40] G.B. Wang, K.H. Xie, H.P. Xu, Y.J. Wang, F. Zhao, Y. Geng, Y.B. Dong, Covalent organic frameworks and their composites as multifunctional photocatalysts for efficient visible-light induced organic transformations, Coord. Chem. Rev. 472 (2022) 214774, https://doi.org/10.1016/j.ccr.2022.214774.

[41] P. Das, J. Roeser, A. Thomas, Solar light driven H₂O₂ production and selective oxidations using a covalent organic framework photocatalyst prepared by a multicomponent reaction, Angew. Chem. Int. Ed. 62 (2023) e202304349, https://doi.org/10.1002/anie.202304349.

[42] X.X. Liu, R.L. Qi, S.M. Li, W.R. Liu, Y.Y. Yu, J.H. Wang, S.M. Wu, K.J. Ding, Y. Yu, Triazine-porphyrin-based hyperconjugated covalent organic framework for high-performance photocatalysis, J. Am. Chem. Soc. 144 (2022) 23396–23404, https://doi.org/10.1021/jacs.2c09369.

[43] D. Meng, J. Xue, Y.F. Zhang, T.J. Liu, C.C. Chen, W.J. Song, J.C. Zhao, Covalent organic frameworks editing for efficient metallaphotoredox catalytic carbon–oxygen cross coupling of aryl halides with alcohols, Catal. Sci. Technol. 13 (2023) 1518–1526, https://doi.org/10.1039/d2cy01535h.

[44] Y.H. Kim, J.P. Jeon, Y. Kim, H.J. Noh, J.M. Seo, J. Kim, G. Lee, J.B. Baek, Cobalt-porphyrin-based covalent organic frameworks with donor-acceptor units as photocatalysts for carbon dioxide reduction, Angew. Chem. Int. Ed. 62 (2023) e202307991, https://doi.org/10.1002/anie.202307991.

[45] C.C. Qin, X.D. Wu, L. Tang, X.H. Chen, M. Li, Y. Mou, B. Su, S.B. Wang, C.Y. Feng, J.W. Liu, X.Z. Yuan, Y.L. Zhao, H. Wang, Dual donor-acceptor covalent organic frameworks for hydrogen peroxide photosynthesis, Nat. Commun. 14 (2023) 5238, https://doi.org/10.1038/s41467-023-40991-7.

[46] J.P. Jeon, Y.J. Kim, S.H. Joo, H.J. Noh, S.K. Kwak, J.B. Baek, Benzotrithiophene-based covalent organic framework photocatalysts with controlled conjugation of building blocks for charge stabilization, Angew. Chem. Int. Ed. 62 (2023) e202217416, https://doi.org/10.1002/anie.202217416.

[47] S.X. Li, R. Ma, S.Q. Xu, T.Y. Zheng, G.E. Fu, Y.L. Wu, Z.Q. Liao, Y.B. Kuang, Y. Hou, D.S. Wang, P.S. Petkov, K. Simeonova, X.L. Feng, L.Z. Wu, X.B. Li, T. Zhang, Direct construction of isomeric benzobisoxazole–vinylene-linked covalent organic frameworks with distinct photocatalytic properties, J. Am. Chem. Soc. 144 (2022) 13953–13960, https://doi.org/10.1021/jacs.2c06042.

[48] D.L. Jiang, Covalent organic frameworks: An amazing chemistry platform for designing polymers, Chem 6 (2020) 2461–2483, https://doi.org/10.1016/j.chempr.2020.08.024.

[49] T. Banerjee, F. Podjaski, J. Kröger, B.P. Biswal, B.V. Lotsch, Polymer photocatalysts for solar-to-chemical energy conversion, Nat. Rev. Mater. 6 (2021) 168–190, https://doi.org/10.1038/s41578-020-00254-z.

[50] Y.H. Kim, N. Kim, J.M. Seo, J.P. Jeon, H.J. Noh, D.H. Kweon, J. Ryu, J.B. Baek, Benzothiazole-based covalent organic frameworks with different symmetrical combinations for photocatalytic CO₂ conversion, Chem. Mater. 33 (2021) 8705–8711, https://doi.org/10.1021/acs.chemmater.1c02660.

[51] J.Y. Yue, L.P. Song, Y.F. Fan, Z.X. Pan, P. Yang, Y. Ma, Q. Xu, B. Tang, Thiophene-containing covalent organic frameworks for overall photocatalytic H₂O₂ synthesis in water and seawater, Angew. Chem. Int. Ed. 62 (2023) e202309624, https://doi.org/10.1002/anie.202309624.

[52] J.Y. Chen, Y.Y. Jiang, J. Yang, Y.L. Sun, L.X. Shi, Y. Ran, Q.S. Zhang, Y.P. Yi, S. Wang, Y.L. Guo, Y.Q. Liu, Copolymers of bis-diketopyrrolopyrrole and benzothiadiazole derivatives for high-performance ambipolar field-effect transistors on flexible substrates, ACS Appl. Mater. Interfaces 10 (2018) 25858–25865, https://doi.org/10.1021/acsami.7b16516.

[53] L.P. Guo, S.B. Jin, Stable covalent organic frameworks for photochemical applications, ChemPhotoChem 3 (2019) 973–983, https://doi.org/10.1002/cptc.201900089.

[54] H.L. Yu, P.K. Zhou, X. Chen, Intramolecular hydrogen bonding interactions induced enhancement in resistive switching memory performance for covalent organic framework-based memristors, Adv. Funct. Mater. 33 (2023) 2308336, https://doi.org/10.1002/adfm.202308336.

[55] J. Cheng, Y.T. Wu, W. Zhang, J. Zhang, L. Wang, M. Zhou, F.T. Fan, X.J. Wu, H. X. Xu, Fully conjugated 2D sp² carbon-linked covalent organic frameworks for photocatalytic overall water splitting, Adv. Mater. 36 (2024) 2305313, https://doi.org/10.1002/adma.202305313.

[56] W.B. Chen, L. Wang, D.Z. Mo, F. He, Z.L. Wen, X.J. Wu, H.X. Xu, L. Chen, Modulating benzothiadiazole-based covalent organic frameworks via halogenation for enhanced photocatalytic water splitting, Angew. Chem. Int. Ed. 59 (2020) 16902–16909, https://doi.org/10.1002/anie.202006925.

[57] X. Li, S.X. Yang, F.L. Zhang, L.Y. Zheng, X.J. Lang, Facile synthesis of 2D covalent organic frameworks for cooperative photocatalysis with TEMPO: The selective aerobic oxidation of benzyl amines, Appl. Catal. B 303 (2022) 120846, https://doi.org/10.1016/j.apcatb.2021.120846.

[58] G.H. Wu, Y.H. Zhang, R. Kaneko, Y. Kojima, Q. Shen, A. Islam, K. Sugawa, J. Otsuki, A 2,1,3-benzooxadiazole moiety in a D–A–D-type hole-transporting material for boosting the photovoltage in perovskite solar cells, J. Phys. Chem. C 121 (2017) 17617–17624, https://doi.org/10.1021/acs.jpcc.7b04614.

[59] Z.J. Wang, S. Ghasimi, K. Landfester, K.A.I. Zhang, Molecular structural design of conjugated microporous poly(benzooxadiazole) networks for enhanced photocatalytic activity with visible light, Adv. Mater. 27 (2015) 6265–6270, https://doi.org/10.1002/adma.201502735.

[60] T.T. Do, K. Matsuki, T. Sakanoue, F.L. Wong, S. Manzhos, C.S. Lee, J. Bell, T. Takenobu, P. Sonar, Indenofluorene-based-copolymers: Influence of electron-deficient benzothiadiazole (BT) and benzooxadiazole (BO) moieties on light emitting devices, Org. Electron. 70 (2019) 14–24, https://doi.org/10.1016/j.orgel.2019.03.050.

[61] F.L. Zhang, K.H. Xiong, X.J. Lang, Two-dimensional β-ketoenamine-linked covalent organic frameworks for visible light photocatalysis, ChemCatChem 15 (2023) e202301179, https://doi.org/10.1002/cctc.202301179.

[62] N.Y. Huang, Y.T. Zheng, D. Chen, Z.Y. Chen, C.Z. Huang, Q. Xu, Reticular framework materials for photocatalytic organic reactions, Chem. Soc. Rev. 52 (2023) 7949–8004, https://doi.org/10.1039/d2cs00289b.

[63] L.Q. Xiong, J.W. Tang, Strategies and challenges on selectivity of photocatalytic oxidation of organic substances, Adv. Energy Mater. 11 (2021) 2003216, https://doi.org/10.1002/aenm.202003216.

[64] P. Pachfule, A. Acharjya, J. Roeser, T. Langenhahn, M. Schwarze, R. Schomäcker, A. Thomas, J. Schmidt, Diacetylene functionalized covalent organic framework (COF) for photocatalytic hydrogen generation, J. Am. Chem. Soc. 140 (2018) 1423–1427, https://doi.org/10.1021/jacs.7b11255.

[65] B.P. Biswal, H.A. Vignolo-González, T. Banerjee, L. Grunenberg, G. Savasci, K. Gottschling, J. Nuss, C. Ochsenfeld, B.V. Lotsch, Sustained solar H₂ evolution from a thiazolo[5,4-d]thiazole-bridged covalent organic framework and nickel-thiolate cluster in water, J. Am. Chem. Soc. 141 (2019) 11082–11092, https://doi.org/10.1021/jacs.9b03243.

[66] T. Zhou, L. Wang, X.Y. Huang, J. Unruangsri, H.L. Zhang, R. Wang, Q.L. Song, Q. Y. Yang, W.H. Li, C.C. Wang, K. Takahashi, H.X. Xu, J. Guo, PEG-stabilized coaxial stacking of two-dimensional covalent organic frameworks for enhanced photocatalytic hydrogen evolution, Nat. Commun. 12 (2021) 3934, https://doi.org/10.1038/s41467-021-24179-5.

[67] X.J. Li, H. Huang, H.J. Bin, Z.X. Peng, C.H. Zhu, L.W. Xue, Z.G. Zhang, Z.J. Zhang, H. Ade, Y.F. Li, Synthesis and photovoltaic properties of a series of narrow bandgap organic semiconductor acceptors with their absorption edge reaching 900 nm, Chem. Mater. 29 (2017) 10130–10138, https://doi.org/10.1021/acs.chemmater.7b03928.

[68] Z.F. Zhao, Y.L. Zheng, C. Wang, S.N. Zhang, J. Song, Y.F. Li, S.Q. Ma, P. Cheng, Z. J. Zhang, Y. Chen, Fabrication of robust covalent organic frameworks for enhanced visible-light-driven H₂ evolution, ACS Catal. 11 (2021) 2098–2107, https://doi.org/10.1021/acscatal.0c04820.

[69] Y.L. Yang, N. Luo, S.Y. Lin, H. Yao, Y.Q. Cai, Cyano substituent on the olefin linkage: Promoting rather than inhibiting the performance of covalent organic frameworks, ACS Catal. 12 (2022) 10718–10726, https://doi.org/10.1021/acscatal.2c02908.

[70] F.W. Huang, Y.X. Wang, X.Y. Dong, X.J. Lang, Merging benzotrithiophene covalent organic framework photocatalysis with TEMPO for selective oxidation of organic sulfides, Sci. China Chem. 66 (2023) 3290–3296, https://doi.org/10.1007/s11426-023-1644-x.

[71] E. Skolia, P.L. Gkizis, C.G. Kokotos, Aerobic photocatalysis: oxidation of sulfides to sulfoxides, ChemPlusChem 87 (2022) e202200008, https://doi.org/10.1002/cplu.202200008.

[72] F.L. Zhang, X.M. Ma, X.Y. Dong, X. Miao, X.J. Lang, Inserting acetylene into an olefin-linked covalent organic framework for boosting the selective photocatalytic aerobic oxidation of sulfides, Chem. Eng. J. 451 (2023) 138802, https://doi.org/10.1016/j.cej.2022.138802.

[73] F.L. Zhang, Y.X. Wang, H.X. Zhao, X.Y. Dong, X.K. Gu, X.J. Lang, Expanding olefin-linked covalent organic frameworks toward selective photocatalytic oxidation of organic sulfides, ACS Appl. Mater. Interfaces 16 (2024) 8772–8782, https://doi.org/10.1021/acsami.3c16838.

[74] R.L. Jensen, J. Arnbjerg, P.R. Ogilby, Temperature effects on the solvent-dependent deactivation of singlet oxygen, J. Am. Chem. Soc. 132 (2010) 8098–8105, https://doi.org/10.1021/ja101753n.